INSTRUMENTATION

A Gamma Camera for Medical Applications, using a Multiwire Proportional Counter

Jeffrey L. Lacy, Adrian D. LeBlanc, John W. Babich, Michael W. Bungo, Larry A. Latson, Robert M. Lewis, Larry R. Poliner, Robert H. Jones, and Philip C. Johnson

NASA-Johnson Space Center and Baylor College of Medicine, Houston, Texas, and Duke University Medical Center, Durham, North Carolina

A multiwire proportional counter gamma camera, specifically designed for nuclear medicine applications, is portable and weighs less than 50 lb including shielding and collimator. The basic operating characteristics have been investigated with various radioactive sealed sources. The camera demonstrates a peak count rate of 850,000 cps, an intrinsic spatial resolution of 2.5 mm, and excellent image uniformity when used with x-ray sources in the range of 22–81 keV. Tests of the device with Ta-178—a very promising, short half-life (9.3 min), low-energy radionuclide—using 20 mCi injections provided images of quality comparable to those obtained from 15 mCi Tc-99m studies with conventional imaging devices. The camera used with Ta-178 offers particular promise in first-pass nuclear cardiology studies. Considerably improved study quality will likely result in this area because of the increased injectable dose levels offered by Ta-178 combined with the high-count rate capability and improved resolution.

J Nucl Med 25: 1003–1012, 1984

The multiwire proportional counter (MWPC) was developed in the late 1960s for applications in high-energy physics (*1*,*2*). Since that time, MWPC technology has developed rapidly and is currently heavily utilized in this field for position determination of particles and gamma rays. Although widespread use of the MWPC as a medical imaging device has not yet emerged, the potential is well recognized (*3*).

A number of groups have developed and reported MWPC single-photon imaging detectors (*4–6*). Reported devices using moderate pressurization (<5 atmospheres) have shown good resolution, simplicity of construction, and generally good results for detection of radiation in the energy range 20–80 keV. One group has described a 10-atmosphere device and its use with Tc-99m (*5*). Significant difficulties were reported, including problems with fluorescence emission, rapid gas contamination, and signal rise-time fluctuations.

A deficiency of all reported devices is the inability of their basic electronic systems to form images at the high counting rates that are made possible by the basic MWPC detector. The potential high-count-rate capability is a feature that should be used to advantage in dynamic radionuclide studies.

We report a MWPC camera of moderate pressurization that allows nearly full realization of the device's basic advantages. The camera exceeds the state of the art in nuclear medicine imaging in both count-rate capability and spatial resolution. Furthermore, its images are almost totally free of the distortions often present in Anger camera images, particularly at high count rates. The camera is also very compact, lightweight, and capable of portable operation.

Detection efficiency limits the application of the device to energies below 100 keV. Although the most commonly used radionuclide, Tc-99m, cannot be ade-

Received June 1, 1983; revision accepted Apr. 18, 1984.

For reprints contact: Jeffrey L. Lacy, PhD, The Methodist Hospital, MSF905, 6565 Fannin, Houston, TX 77030.

TABLE 1. CAMERA PHYSICAL CHARACTERISTICS

Sensitive area	25 cm diameter
Sensitive depth	5 cm
Gas mixture	90% xenon, 10% methane
Gas pressure	3–5 atmospheres
Wire spacing	2 mm anode and cathode
Anode-cathode spacing	6 mm
Entrance window	0.51 mm aluminum
Total camera weight	23 kg
External dimensions	40 × 40 × 12 cm

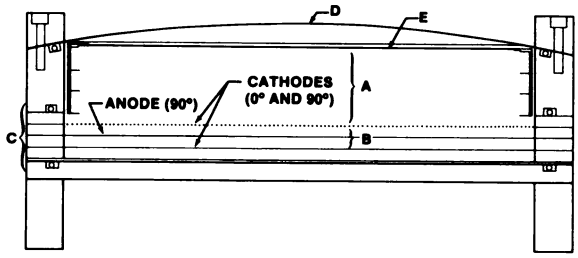

FIG. 1. Longitudinal diagram of MWPC detector showing: drift region (A), detection region (B), aluminum pressure vessel (C), aluminum entrance window (D), and negative high-voltage collection electrode (E).

quately imaged, there are significant areas of application of the camera. The commercially available emitters Tl-201 and Xe-133 both should be excellently imaged by the MWPC. A newly reported radionuclide, Ta-178, (*7–9,11*) has very promising potential as a cardiac imaging agent (*9*). Its short half-life offers significant advantages over Tc-99m, and its energy (55–65 keV) is ideally suited to the MWPC. A suitable generator system has been developed (*8*) and is used extensively in our laboratory. Full development of Ta-178 into a routinely available radionuclide, along with the commercial nuclides mentioned, would provide a powerful radionuclide inventory for use with the MWPC.

We present here detailed tests of the camera system, covering many of the characteristics important to application in nuclear medicine. In this paper we limit ourselves to results with the radionuclides Ta-178, Am-241, I-125, Xe-133, and Cd-109. Detailed performance with Tl-201 and Xe-133 is being explored and will be reported in the future. In addition, we present initial physiological testing of the camera with Ta-178 in animals. In this testing we have concentrated on the first-pass radionuclide ventriculography technique. Samples of these studies carried out in the dog and pig are presented.

INSTRUMENT DESCRIPTION

The MWPC detector produces a signal whose duration is one-tenth that of NaI(Tl). All commercially available instrumentation for radionuclide imaging is based on NaI(Tl), and its slow pulses significantly limit the rate at which position information can be collected. We have developed a detector and electronics that take almost full advantage of the intrinsic speed of the MWPC while maintaining a simple physical and electronic design that is compatible with low cost.

The basic physical characteristics of the detector are summarized in Table 1. A longitudinal section is shown in Fig. 1. The detector consists of a drift region (A) and a detection region (B), contained within an aluminum pressure vessel (C) having a thin aluminum entrance window of spherical shape (D).

X-rays entering through the aluminum window interact with the pressurized gas (xenon) in region A. The resulting ions are impelled to the detection region by a drift field of 1000 volts/cm. In the detection region are mounted three parallel wire planes: two outer planes being operated at ground potential (cathodes), with the inner plane at high positive potential (anode). The drifted ionization is collected at the anode, where the charge is amplified by gas avalanche.

Position determination of the anode avalanche is obtained by detection of the signals induced in the two cathode grids, which are oriented orthogonally to each other. Each wire of each cathode grid is attached to a tap of a discrete delay line, and position is sensed by measurement of the delay time between occurrence of the avalanche on the anode grid and arrival of the signals at the ends of the cathode delay lines. Unlike previously reported delay-line readout systems for medical applications (*4*), we use very high-speed delay lines (delay = 10 nsec/cm) (*10*). This provides a maximum delay-line clearance time of less than 250 nsec and a typical mean clearance time of 150 nsec. Therefore, rate performance is improved with this system.

The encoding of the position of an event is accomplished through high-speed digital circuitry. The electronic block diagram is shown in Fig. 2. The four time delays obtained from the delay lines are digitized by high-speed counters (600 MHz), which are gated by the anode signal and gated off by the delay-line outputs. These four digital values are passed on to a high-speed processing unit that forms the digital sum of the coordinates obtained from a given delay line. This sum value is compared with a constant value equal to the total delay of the delay line. This test rejects any confused events that result from pile-up or scatter within the detector gas. Energy selection is accomplished by application of a pulse-height window test to the prompt anode signal. If this test is failed, the digital counters are not started and the circuits are immediately ready to process a new event.

Simultaneously with the sum test, the processor also computes a difference between the delays on each axis

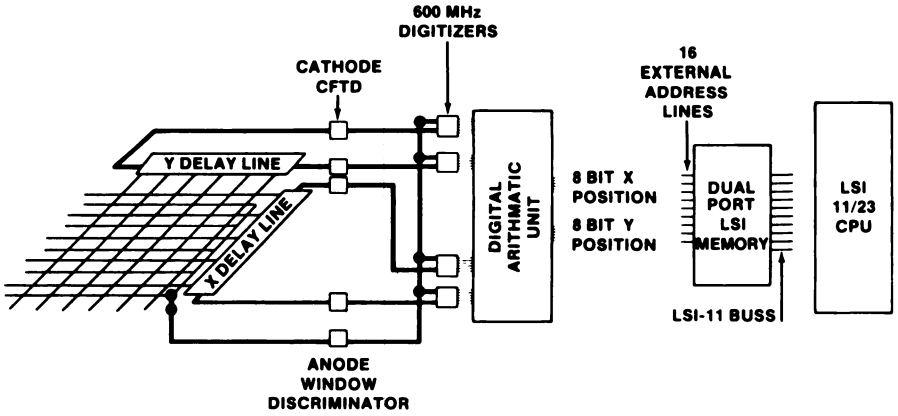

FIG. 2. Block diagram of readout electronics.

and adds a digital offset value. This value for each axis (8-bit words) is used as the event position (for zero offset it is the position relative to the center of the chamber). The digital sum and difference logic is implemented with high-speed, Motorola emitter coupled logic (MECL) circuits that require less than 300 nsec to perform the sum test and to provide the difference position value.

The offset difference values (8 bits X and 8 bits Y) are passed through a formatting circuit that sets the desired frame format. Four frame sizes are facilitated—16 × 16, 32 × 32, 64 × 64, and 128 × 128. In each of these formats the cell size can be zoomed by factors of 2 and 4. A continuous zoom capability is also provided by variation of oscillator frequency, which can range from 100–600 mHz, providing a continuous zoom by a factor of 6.

The formatted digital position coordinates are transferred through a first in, first out (FIFO) memory into an LSI-11/23 computer by means of a unique dual-ported memory. This memory can respond on the LSI-11 buss as a standard RAM memory, or under software control can be set to respond on an external buss to the digital coordinates from the arithmetic processor. The memory can accept events on the external buss at a rate of 3 MHz.

The LSI-11 computer controls data acquisition, display, and storage. Data can be stored either on a flexible disk (RX02) or hard disk (RK05). A color display system is used for image display of both processed and real-time images. Static image data can be collected and stored to disk. Dynamic study data can be collected and written to RK05 disk in film-strip fashion. Frames of 64 × 64 pixels can be collected at 10 fps, 32 × 32 frames at 40 fps, and 16 × 16 frames at 160 fps. The image memory of the display system can be used as a high-speed image buffer memory. The 256 × 256 pixel memory allows storage of up to 64k bytes of acquired image data. Dynamic image data can be collected in this buffer at approximately four times the rate allowed by the RK05 disk. The LSI-11/23 also provides a powerful postdata-collection processing system.

BASIC PERFORMANCE CHARACTERISTICS

Efficiency and sensitivity. The absolute detection efficiency of the detector operated at 3 and 5 atmospheres (absolute) is plotted in Fig. 3. The efficiencies at the energies of the potentially useful nuclides I-125, Ta-178, Tl-201, and Xe-133 are indicated. Thorough pressure testing of the camera indicates that it can be operated safely at pressures up to 5 atm (safety factor of 4). Although operation at this pressure would significantly increase detection efficiencies, particularly for Tl-201 and Xe-133, we have chosen to explore thoroughly the capabilities of the device at 3 atm before going to higher pressures. All results reported here were obtained at 3 atm (absolute).

Energy resolution. The energy deposition mechanism in a MWPC is dependent on the energy of the incident photon. For energies below the K-shell excitation energy of xenon (35 keV), L-shell interactions occur and most of the photon energy is deposited entirely at the interaction site. For energies above 35 keV, the excess energy above 35 keV is deposited at the interaction site and a 30-keV fluorescence photon is emitted 88% of the time

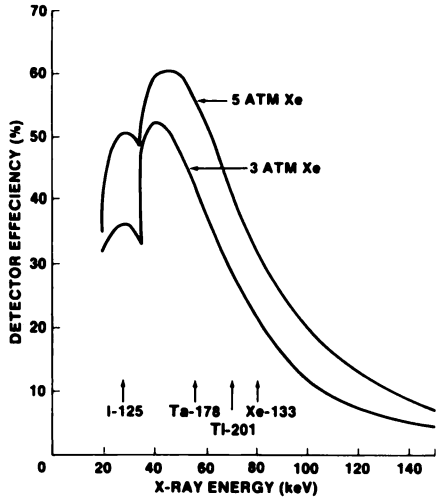

FIG. 3. Detector efficiency against x-ray energy for operating pressures of 3 and 5 atmospheres absolute.

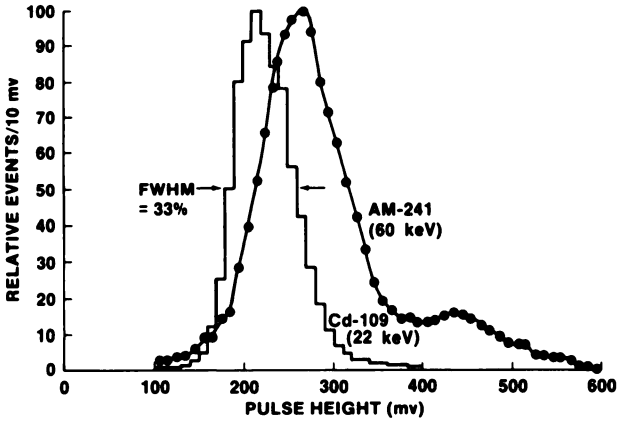

FIG. 4. Pulse-height spectra of Cd-109 (22 keV) and Am-241 (60 keV). Deposited energies in these cases are 22 and 25 keV respectively.

(12% of the fluorescence emissions are internally converted, leading to total energy deposition at the interaction site).

To demonstrate the energy resolution characteristics of the MWPC, we display in Fig. 4 the energy spectrum of Cd-109 and Am-241. Cd-109 emits dominantly 22 keV x-rays (Ag K x-rays) and a very low abundance (3%) 88 keV photon, whereas Am-241 emits only a 60 keV photon. Thus, these two nuclides produce 22-keV and 25-keV deposited energy (with 30-keV fluorescence escape in the case of Am-241). Due to the dominance of fluorescence escape in our detector design, the intrinsic energy resolution for 60-keV x-rays from Fig. 4 is 33% of 25 keV, or 14% (FWHM) of the total incident energy. This is the energy-resolution figure that should be used for comparisons with NaI devices which have negligible fluorescence escape. Although this value is roughly equivalent to NaI devices, we expect significant improvement in the future through modifications in the pulse-height measurement circuitry. The current circuits use only the leading edge (first 30 nsec) of the proportional charge collected, which probably does not contain an adequate portion of the charge delivered. The likely enhanced energy resolving power in the 50- to 80-keV range could be significant in rejection of Compton scatter at these low energies.

An idiosyncrasy resulting from flourescence escape should be discussed. An x-ray, such as that from Ta-178, which is 25 keV above the xenon K-shell energy, is indistinguishable from x-rays of 25 keV total incident energy, since the latter are below the xenon K shell. Thus, an energy window set to accept 50–70 keV x-rays, as might be done for Ta-178 imaging, will also accept Compton degraded x-rays in the energy range 15–35 keV. This is of little practical consequence, since very little of the Compton radiation is able to scatter down from 60 keV to 35 keV and penetrate intervening tissue. What little flux may be present in this energy range can be very effectively removed with a copper filter. This effect would be a problem only for nuclides with emissions much closer to the K-shell energy.

Gas contamination is a well-known phenomenon in long-term sealed operation of MWPC detectors. Electronegative gas contaminants, which can result from outgassing of detector interior structure, cause loss of primary ionization produced by x-ray interactions. Effects of such contaminants show up as a spreading of the detector's energy resolution. To evaluate this potential problem, the Cd-109 pulse-height spectrum was carefully monitored for loss of resolution over a period of 90 days. No discernible deterioration occurred over this period. Thus, gas contamination is not expected to be a significant operational problem. Contamination tests of longer duration are in progress.

Rate performance. The event-rate performance of the camera was investigated by irradiation of the uncollimated camera with a 40-mCi Am-241 source. In Fig. 5 various rates are plotted against the distance of this source from the camera. The image rate curve (C) shows the paralyzing behavior typical of both Anger and multicrystal cameras, with a peak count rate of 850,000 cps. At this peak count rate approximately 50% of the

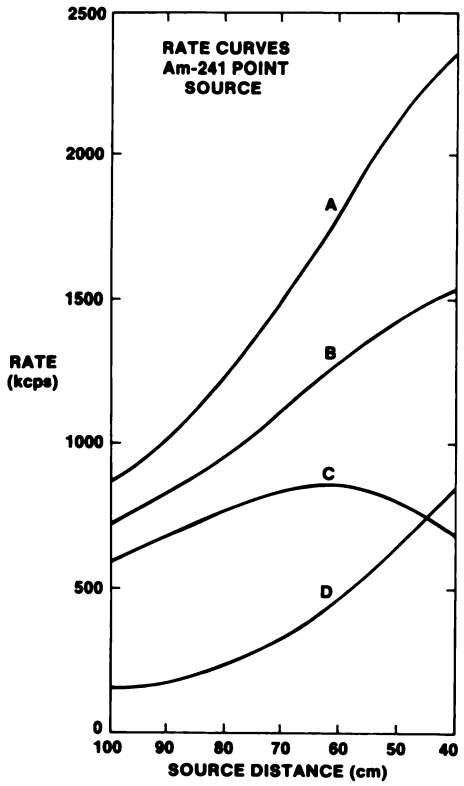

FIG. 5. Detector rates for uncollimated detector irradiated by Am-241 source, against distance of source from face of detector. A = threshold discriminator count rate. B = window discriminator count rate (30% window). C = count rate passing energy window and ambiguity rejection circuitry. D = rate of rejection by ambiguity circuitry.

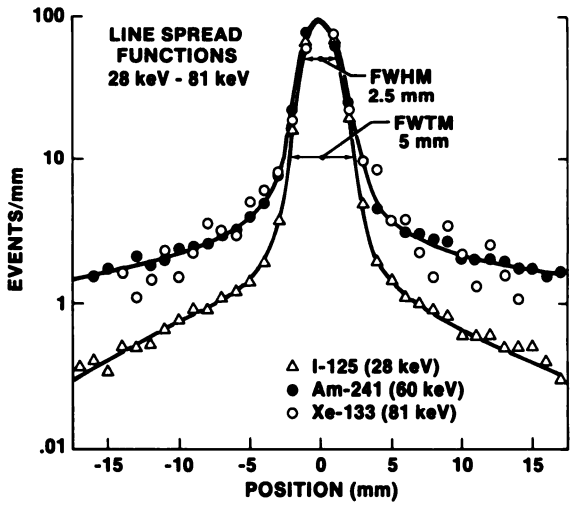

FIG. 6. Line spread functions for Am-241 (60 keV), I-125 (28 keV), and Xe-133 (81 keV). For Xe-133 a 1-mm Cu absorber was used to remove abundant xenon fluorescence x-rays.

events interacting in the detector make it through the digitizing circuitry into the image. Curve A is the anode discriminator rate; curve B the rate at which events pass the energy window; and curve D is the rate of event rejection by the sum test logic.

Intrinsic detector resolution and image uniformity. The intrinsic detector resolution was determined by irradiation of the detector along a narrow line (<1 mm width). Figure 6 shows the line spread functions measured in this way for x-ray energies of 28, 60, and 81 keV. The resolution at 28 keV determined by this technique is 2.5 mm full width half maximum (FWHM) and 5 mm full width tenth maximum (FWTM). These values are degraded by less than 5 percent for 60-keV and 81-keV x-rays.

As previously indicated, most of the detected events in the MWPC are events for which fluorescence escape has occurred. Fluorescence photons have a large mean range in the gas (11 cm). Thus, in the small percentage of cases that these x-rays interact, they can significantly alter the measured x-ray position. The effect of fluorescence on resolution can be quantified by comparing the 60-keV and 81-keV line spread functions with that for 28-keV x-rays from I-125 (Fig. 6). The latter do not excite fluorescence. The FWHM and FWTM values are only very slightly degraded by the presence of this radiation; however, the effect of fluorescence shows up in two subtle ways. First, there is a low-level halo effect, which appears as a small tail in Fig. 6. It results from clean detection of a fluorescence photon, usually many cm from the interaction site. Second, a higher sum-test rejection rate is observed for the 60-keV radiation. At low event rates, a rejection rate of 13% is observed for 60 keV whereas 3% is observed for 22 keV. These measurements show that very small effects on image quality result from the fluorescence. The effect is limited to a slight reduction in sensitivity (10%) and a very low-level, diffuse halo. Most of the events with associated fluorescence interactions are rejected by the sum-test logic.

Image uniformity was investigated by irradiation of the uncollimated detector with an Am-241 source at a distance of 1.5 meters. The resulting flood image is shown in Fig. 7A for a pixel resolution of 2 × 2 mm. Uniformity fluctuations of at most ±5% are present.

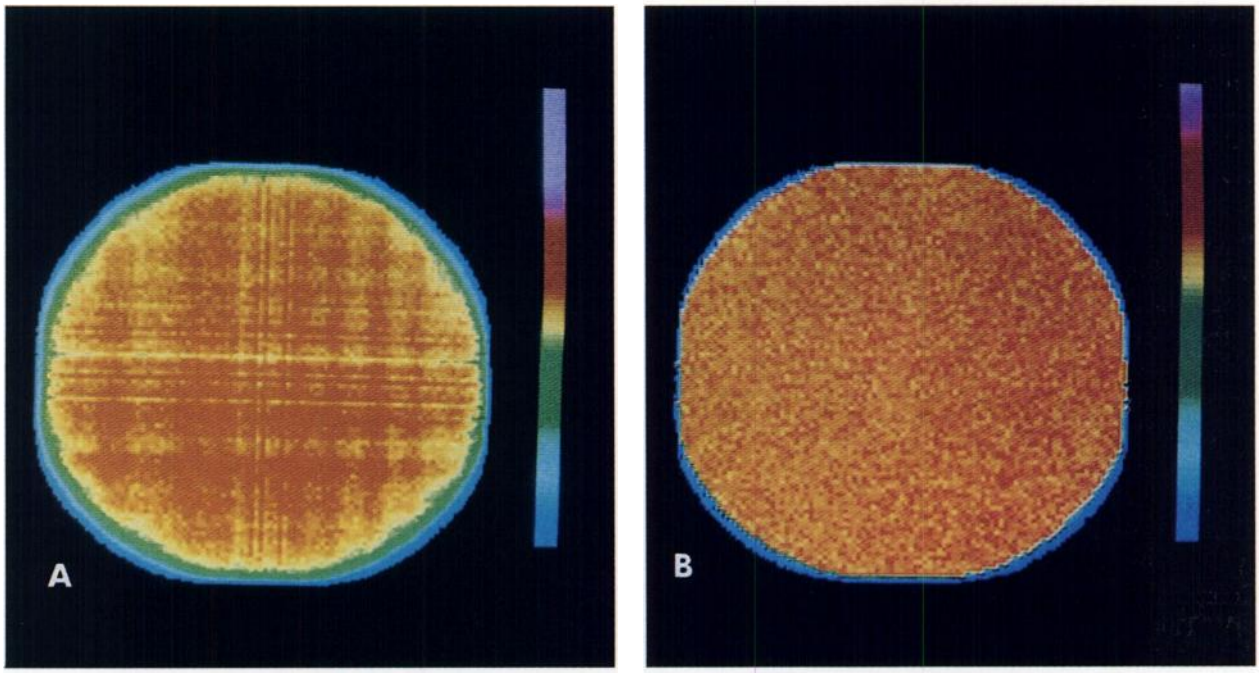

FIG. 7. A: Am-241 flood image obtained by irradiation of uncollimated detector at 1.5 m distance; 128 × 128 format with 2 × 2 mm cell size. B: corresponding flood-corrected image.

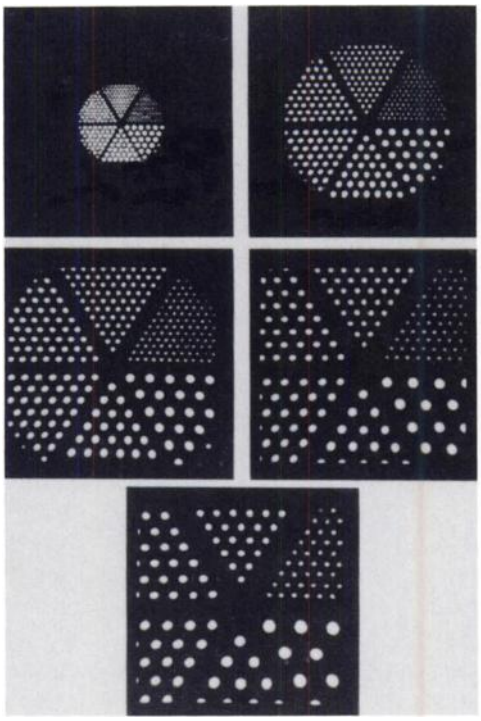

FIG. 8. Anger pie-phantom images for oscillator frequencies of 100, 200, 300, 400, and 500 MHz.

Most of the nonuniformity is confined to very-high-frequency fluctuations within a spatial scale of less than 3 mm. These likely result from differential nonuniformities of the delay lines used for readout and from slight variations in detector wire spacing. The nonuniformities have been shown to be both stable and correctable. Figure 7B is a "flood corrected" flood image in which the nonuniformities have been reduced to less than ±1% by flood correction. In many applications such as cardiac imaging, in which high spatial resolution (<5 mm FWHM) is not required, such correction is not necessary.

In order to compare the overall image quality of the MWPC with that of the Anger camera, we have performed standard phantom testing. Figure 8 shows a series of images obtained by irradiation of the uncollimated detector through a standard Anger pie phantom. An Am-241 source was used at a distance of 1.5 m. The zoom effect in these images was obtained by varying the digitizer oscillator frequency from 100 to 500 MHz in 100-MHz steps. The images were collected in 128 × 128 format, with the cell size ranging from 1 × 1 mm for the 500-MHz image to 5 × 5 mm for the 100-MHz image.

FIG. 9. Image of Smith orthogonal hole phantom obtained with Am-241 source at 1.5 m distance and detector event rate of 100,000 cps.

Image distortions were investigated by irradiation of the detector through a standard Smith orthogonal hole phantom (0.63-cm spaced grid of holes 0.16 cm in diameter). An Am-241 source was used at a distance of 1.5 m. Figure 9 shows the resulting image, obtained in 128 × 128 format, 1 × 1 mm cell size, with a detector count rate of 100,000 cps.

Imaging with parallel-hole collimators. Two conventional parallel square-hole collimators have been used with the MWPC camera. Their characteristics are shown in Table 2. Most of the studies reported used the high-sensitivity (HS) collimator, which was chosen to provide adequate resolution and high sensitivity for dynamic cardiac studies. This collimator has an intrinsic sensitivity more than twice that of the Baird 1.5″ collimator and smaller angular acceptance by a factor of 0.77. This collimator's higher sensitivity more than offsets the lower efficiency of the MWPC relative to NaI(Tl). This is a result of the much lower packing fraction of the conventional collimator optimized for low energies, as compared with the Baird collimator, which has very thick septa (*12*).

The sensitivity of the detector operated at 3 atm, measured for the high-sensitivity and high-resolution (HR) collimators, is shown in Table 3 for I-125 and Ta-178 emitters. The calculated sensitivities for Tl-201 and Xe-133 are also included.

The image count rate relative to the Ta-178 dose has

TABLE 2. COLLIMATOR CHARACTERISTICS—CONVENTIONAL SQUARE HOLE

Collimator	Hole length (cm)	Hole size (cm)	Septal thickness (cm)	Sensitivity
High resolution (HR)	2.2	0.14	0.018	9050 cps/mCi
High sensitivity (HS)	1.1	0.14	0.018	36200 cps/mCi

TABLE 3. INSTRUMENT SENSITIVITY IN cps/mCi FOR VARIOUS EMITTERS

Collimator	I-125	Ta-178	Tl-201	Xe-133
High resolution (HR)	3700	3710	2830	2125
High sensitivity (HS)	15000	14900	11351	8513

been determined. A 3-in.-diam beaker containing 70 mCi of Ta-178 in water solution was placed 3 in. above the face of the camera with the HS collimator in place, and the event rate in the detector recorded for a 30-minute period (>3 half-lives). The resulting dose-response curve is plotted in Fig. 10.

The resolution performance of the MWPC camera, using the HS and HR collimators, has been investigated using an Am-241 source 2 mm in diameter. The point spread functions were obtained for various distances between source and collimator in air and in a water bath 15 cm deep. The FWHMs from these point spread functions are plotted in Fig. 11. Note that although much of the Compton-scattered radiation is detected due to the small energy loss in a single Compton interaction at 60 keV, it has very little effect on FWHM. This is doubtless because the Compton angular distribution at 60 keV is nearly isotropic. Thus, much of the scatter entering the collimator is relatively far from the source, resulting in a diffuse halo.

Increased attenuation losses is a concern often expressed with regard to application of low-energy emitters. It is important to realize, however, that the differences between 140 keV and 60 keV is of minimal significance in many applications. The mass attenuation coefficients of soft tissue at these two energies are 0.154 cm^2/g and 0.204 cm^2/g, respectively. At tissue depths

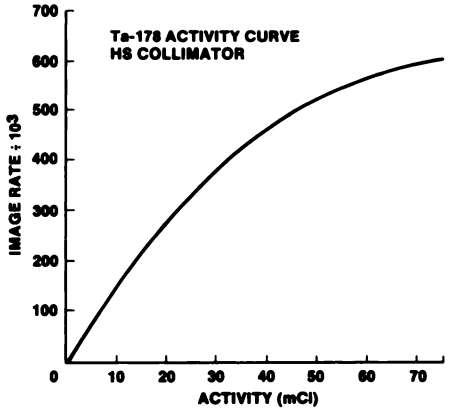

FIG. 10. Detector image rate produced by decaying Ta-178 solution in 7.5 cm beaker, placed 7.5 cm above MWPC camera with HS collimator.

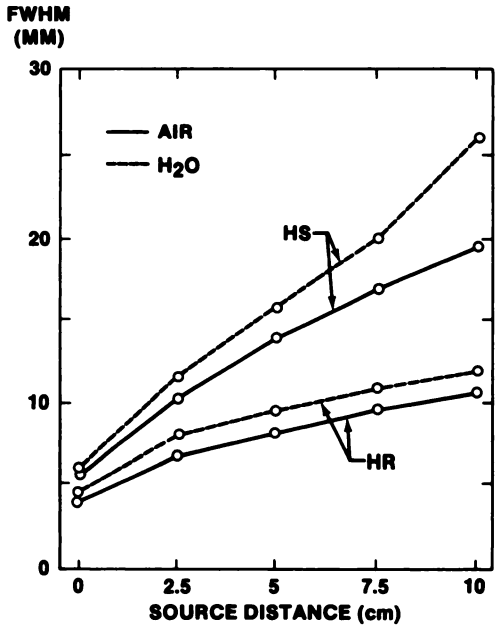

FIG. 11. FWHM plotted against distance to Am-241 point source, in air and H_2O, with HR and HS collimators.

typically encountered in cardiac imaging (5–10 cm), 60 keV produces a transmitted flux of 73% of that produced by an equal 140-keV dose. Only for deep-organ imaging (>10 cm depth) are image statistics significantly affected by 60-keV x-ray energy compared with Tc-99m. For example, at a 15-cm depth, 60-keV radiation is attenuated to 47% of that of 140-keV radiation. Bone attenuation is another potential concern. To evaluate the effect of sternum and rib attenuation upon cardiac images, we have measured the total attenuation of 60-keV radiation in human cadaver dry specimens. In the anterior and left anterior oblique projections, the total sternal attenuation in an average subject was found to be less than 4%, and the rib attenuation less than 3%. These values are below the statistical noise level in typical cardiac images, and therefore should be of little consequence.

ANIMAL CARDIAC STUDIES

First-pass radionuclide ventriculography studies have been carried out in animal subjects in order to determine the effectiveness of the MWPC camera and Ta-178 combination in a common dynamic study. We used a 32-kg dog and a 68-kg pig. Several studies were performed in each subject at short repeat intervals to determine the reproducibility of ejection fraction and wall-motion measurements. Images were evaluated for overall quality. For comparison, a study was carried out in a pig using Tc-99m and a multicrystal camera*. All MWPC studies used the high-sensitivity collimator, whereas a standard 1″ collimator was used with the camera.

TABLE 4. SUBJECT DATA

Subject number	Species	Weight	Anesthesia	Ta dose	or	Tc dose
1	dog	32 Kg	nembutal	20 mCi		—
2	pig	68 Kg	sodium thiamylal	12 mCi		15 mCi

METHODS

A jugular venous catheter was implanted in each subject to provide for reproducible bolus injection and for convenience in handling the subjects. The catheter was inserted to the junction of the superior vena cava and right atrium. All subjects were anesthetized for the duration of the studies—pentobarbital for the dog and sodium thiamylal for the pig—in titrated amounts to produce sedation but not respiratory arrest. Tantalum-178 was injected in all cases as a 1.5-ml bolus followed by a 10-ml rapid saline flush (<0.5 sec injection time). Technetium-99m was injected as a 0.5-ml bolus followed by a 10-ml flush.

Detailed subject data are shown in Table 4. MWPC image data were collected in a 16 × 16 cell format and 1 cm^2 pixel area. Frame collection was begun just before injection and continued for 20 sec. The frame rate was varied from study to study so that ~16 frames per cardiac cycle were collected. The multicrystal camera study used the standard procedure with 50 fps.

All studies were analyzed to obtain left-ventricular volume curves, ejection fraction, and representative cycle images. Data analysis of the MWPC studies was identical to that of the Baird study with two exceptions. A first-order spatial smoothing was applied to the raw data rather than the temporal smooth, and the left-ventricular phase background subtraction was applied without temporal variation.

Three studies were performed on Subject 1 (Table 4) at 30-min intervals, the first two in the anterior position and the third in left lateral. Subject 2 was studied once in left lateral and once, 1 hr later, in the anterior position. The multicrystal camera comparison studies were performed on this subject 2 hr later, with light anesthesia maintained in the interim. A left lateral study was performed first (15 mCi of Tc-99m) followed 15 minutes later by an anterior study (15 mCi of Tc-99m). A static background was collected between studies and used to subtract background from the second study.

RESULTS

The analyzed left-ventricular images for one anterior and one left-lateral canine study are shown in Fig. 12. The diastolic image border, defined as the point at which the background-subtracted image is 30% of the highest pixel, is shown in white. The color-encoded systolic image is superposed on this border. A second anterior study (not shown) was virtually indistinguishable from the one shown. The calculated ejection fractions for the three studies were 49 and 46% for the two anterior studies and 54% for the left-lateral.

Analyzed left-ventricular images from the pig (Subject 2) are shown in Fig. 13. Ejection fractions of 62% and 68% were found for the anterior and left-lateral views, respectively. A comparison of the left-lateral MWPC study and a similar one on the multicrystal camera is shown in Fig. 14. For ease of comparison, both studies were analyzed on the multicrystal system using identical procedures. The injected doses were 12 mCi (Ta-178) and 15 mCi (Tc-99m). The measured ejection fractions were 62% and 64%.

DISCUSSION

It is evident that the left ventricle is well visualized by this technique. Wall motion is easily determinable. Measurements are repeatable to the extent that the physiologic specimen can be expected to remain stable from study to study.

The MWPC/Ta-178 study compares well with the multicrystal/Tc-99m study. Qualitatively, the images are very similar. Two differences were noted in the data. The total-image statistics for the Ta-178 study were ~30% lower for the same administered dose, and the ventricular cross-sectional area, as determined by standard Baird software, was somewhat increased (25%). The former effect is doubtless a result of the slightly higher attenuation of 60-keV radiation relative to 140 keV. The latter effect probably results from the presence of more background in the Ta-178 study, which is not handled correctly by the standard Baird background subtraction. A separate background technique for Ta-178 will likely be needed for absolute volume measurements.

CONCLUSIONS

The much improved count rate, resolution, and portability of the MWPC detector should lead to significant enhanced capabilities in clinical nuclear medicine applications. The MWPC, however, will have certain optimal areas of application, but in others it will have little

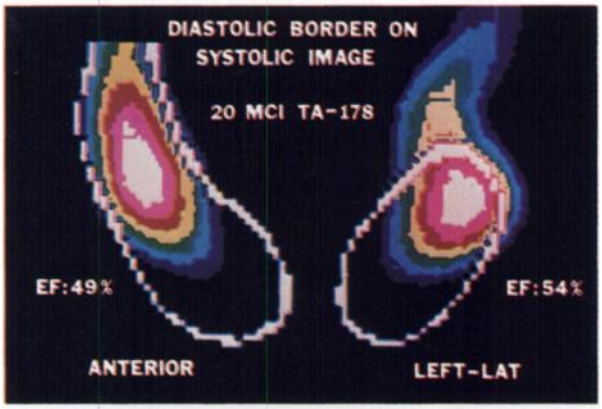

FIG. 12. Representative first-pass study in 32-kg dog, with 20-mCi Ta-178 injection.

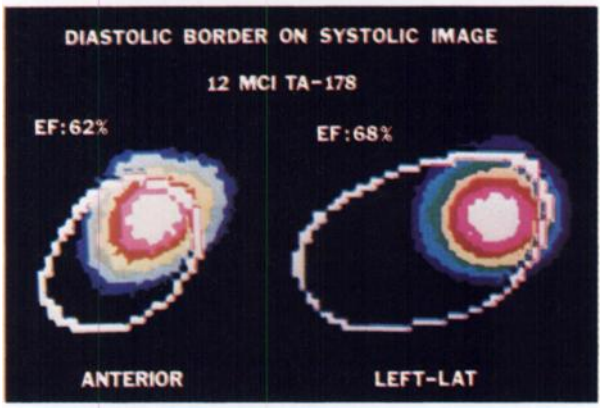

FIG. 13. Representative first-pass study in 68-kg pig, with 12 mCi Ta-178 injection.

or no advantage over existing NaI imaging devices. The limitation of the MWPC to energies below 100 keV makes the imaging of deep organs (>10 cm) difficult due to greater attenuation losses. The concomitant problem with the low-energy limitation, suboptimal scatter rejection, makes it unlikely that the MWPC will compete in photon-deficient applications such as liver imaging. The MWPC should excell, however, in imaging of shallow organs with foci of increased activity, benefiting from high count capability combined with good spatial resolution. Thus, cardiac imaging is a most promising area of application. Many of the limitations in this field currently result from poor counting statistics in first-pass studies and long acquisition times in gated studies. Significant improvement in both of these areas should result from use of the MWPC and Ta-178. They offer whole-body doses a factor of 20 below those with Tc-99m, and critical-organ doses a factor of 65 below those of Tc-99m (*8*). Therefore, much larger doses are possible and multiple studies can also be performed. This, combined with the high count capability of the MWPC, will provide greatly improved image statistics in first-pass studies and lower acquisition times in gated studies. Additional benefits in this field will likely accrue from the compactness of the MWPC, which will allow multiple-head cameras providing simultaneous multiple-view imaging. Single or multiple-head devices with high portability are also possible for application in coronary care units and mobile clinic settings.

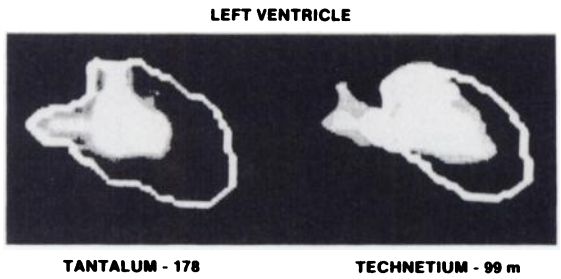

FIG. 14. Comparative study in 68-kg pig. Left: LV image from 12-mCi Ta-178 MWPC first-pass study of Fig. 13, processed by multicrystal camera software. Right: LV image from 15-mCi Tc-99m first-past study carried out and processed on multicrystal system.

Pediatric cardiac applications in particular should benefit greatly from the low radiation exposure of Ta-178. The higher resolution of the MWPC should offer an important enhancement as well in this area, where very high count rates can be achieved over very small spatial dimensions. One can envisage such applications as serial shunt quantitation in which a patient could be studied repeatedly to evaluate shunt status, without catheterization. Also, many forms of anomalous cardiac structure could be assessed with Ta-178 first-pass studies. Yet another application is serial evaluation of the effects of corrective surgery.

Although some of the advantages of Ta-178 could be achieved with NaI devices, cameras currently on the market have significantly compromised performance

with Ta-178 due to high-energy emissions at 0.5 and 1 MeV (*7–8*). These photons penetrate even very-high-energy collimators and are picked up by the NaI crystal with enough efficiency to produce significant deadtime losses (*11*). Although these high-energy gammas penetrate the MGC collimator, they are picked up by the gas detector with far lower efficiency and therefore have little or no effect on deadtime.

Radiology is another field of application for which the MWPC is well suited. Bone densitometry can be carried out by transmission imaging in a fraction of the time required for the scanning techniques, the use of which is increasing. The MWPC has excellent detection characteristics for x-ray energies appropriate for this work (30–80 keV). The high rate capability of the device reported here allows very rapid single-image acquisition, which may be of importance for such applications as osteoporosis screening and diagnosis. This may allow multiple views to be acquired or even tomographic image formation in the same or less time than is required for single-view images using current technology.

Finally, lower instrumentation cost is another potential advantage of the MWPC camera. If mass produced, this device should be cheaper and easier to maintain than sodium iodide devices, and considerably more rugged. The MWPC readout system reported here, being digital in nature, is entirely free from adjustment problems such as those caused by photomultiplier gain drift in crystal cameras.

FOOTNOTE

* Baird System 77.

ACKNOWLEDGMENTS

This work was funded by the NASA Life Sciences Program. Irradiated tantalum foils used for preparation of W-178/Ta-178 generators were kindly supplied by Dr. James Blue under a cooperative agreement with the NASA-Lewis Research Center. We also acknowledge the engineering assistance of the Lockheed Electronics Company, John Saenz and Joseph Kamelgard, and we thank Carole Boney for preparation of the manuscript.

REFERENCES

1. CHARPAK G, et al: The use of multiwire proportional counters to select and localize charged particles. *Nucl Inst Methods* 62:235–240, 1968
2. CHARPAK G, BOUCLIER R, BRESSANI T, et al: Some readout systems for proportional multiwire chambers. *Nucl Inst Methods* 65:217–220, 1968
3. ZIMMERMAN RE: Advances in nuclear medicine imaging instrumentation. In *Medical Radioisotope Scanning.* Vol. 1, pp 121–125, 1976
4. PEREZ-MENDEZ V, KAUFMAN L, LIM CB, et al: Multiwire proportional chambers in nuclear medicine: Present status and perspectives. *J Nucl Med Biol* 3:29–33, 1976
5. BOLON C, et al: Pressurized xenon-filled multiwire proportional chamber for radionuclide imaging. *IEEE Trans Nucl Sci*, NS-25(1):661–664, 1978
6. BORKOWSKI CJ, KOPP MK: Electronic discrimination of the effective thickness of proportional counters. *IEEE Trans Nucl Sci*, NS-24(1):287–292, 1978
7. HOLMAN BL, HARRIS GL, NEIRINCKX RD: Tantalum-178—a short lived nuclide for nuclear medicine: Production of the parent W-178. *J Nucl Med* 19:510–513, 1978
8. NEIRINCKX RD, JONES AG, DARUS MA, et al: Tantalum-178—a-short lived nuclide for nuclear medicine: Development of a potential generator system. *J Nucl Med* 19: 514–519, 1978
9. HOLMAN BL, NEIRINCKX RD, TREVES S, et al: Cardiac imaging with tantalum-178. *Radiology* 131:525–526, 1979
10. LACY JL, LINDSEY RS: High resolution readout of multiwire proportional counters using the cathode coupled delay line technique. *Nucl Inst Methods* 119:483–498, 1974
11. LEBLANC AD, LACY JL, JOHNSON PC, et al: Tantalum-178 count-rate limitations of Anger and multicrystal cameras. *Radiology* 146:242–243, 1983
12. JONES RH, GRENIER RP, SABISTON DC JR: Description of a new high count rate gamma camera system. In *Medical Radioisotopes Scintigraphy*, International Atomic Energy Agency, SM-164/122:299–312, 1973